Scientia Iranica B (2015) 22(2), 448–458

SCIENTIA IRANICA

Sharif University of Technology

Scientia Iranica

Transactions B: Mechanical Engineering

www.scientiairanica.com

Multi-objective optimum stator and rotor stagger angle distributions of an axial turbine stage

A. Asgarshamsi, A. Hajilouy Benisi* and A. Assempour

Department of Mechanical Engineering, Sharif University of Technology, Tehran, P.O. Box 11155-9567, Iran.

Received 6 July 2013; received in revised form 3 April 2014; accepted 4 October 2014

KEYWORDS
Turbine;
Stagger angle;
Optimization;
Stator;
Rotor.

Abstract. Gas turbine aerodynamic shape optimization has been the subject of several numerical studies in the past decades. In this research, numerical optimization of a one stage axial turbine is considered. A practical and effective optimization method to improve efficiency and/or pressure ratio of the axial turbine is presented. Particular modifications are accomplished with a limited number of optimization parameters, by stator and rotor blades re-staggering. A three-dimensional numerical model has been prepared and verified through experimental data, which are obtained from the reference gas turbine engine test rig. Coupling the verified numerical simulation solver and genetic algorithm, the effects of stator and rotor stagger angle distributions on the turbine performance are investigated. The optimization is carried out at the turbine design operating condition. To accelerate the GA convergence rate, the numerical mesh sizes are refined in each generation. As a result, the overall computational time decreases by 20%. Defining two objective functions, this optimization approach resulted in the turbine stage isentropic efficiency improvement of 0.85% and 0.86%, in the first and second objective functions, respectively.

© 2015 Sharif University of Technology. All rights reserved.

1. Introduction

Investigations on gas turbine engine components are performed for developing new products. Since small improvements in performance may result in remarkable saving in operating costs, therefore, aerodynamic optimization is of great importance for the industrial and aerospace applications. Gas turbine performance can be improved by reducing secondary flow, endwalls and blade tip losses [1] or by blade shape improvement. In recent years, the optimization of gas turbine engine components has developed remarkably with rapid enhancement of computational power [2,3]. Automated aerodynamic shape optimization is performed by coupling a sufficiently valid CFD simulation solver with an optimization algorithm to redesign a gas turbine component. Shape optimization in 3D flow can be introduced according to the applications, i.e. axial [4-7] and centrifugal [8,9] compressors, fan [10,11] and turbine blades [3,12-16]. For example, Oyama et al. [4] used evolutionary algorithms in redesign of NASA's Rotor 67. A differential evolution-based optimization algorithm in combination with a NURBS-based parameterization scheme was developed and applied to optimize Rotor 37 by Luo et al. [5]. Arabnia and Ghaly [3] developed a 3D optimization model and applied it for improvement of an axial turbine stage. The optimization strategy obtained around 1% increase in the turbine stage efficiency. This method was the basis for the other papers by the authors [13-15]. Yuan et al. [16] optimized a steam turbine stage considering rotor blade profiles, its lean and twist stacking line and hub end-wall geometry. The objective function was the stage efficiency with a constraint on turbine stage mass flow rate or throat area. The highest efficiency increase was 0.22%.

The main objective of this paper is to employ the

*. *Corresponding author. Tel.: +98 21 66165512*
E-mail address: Hajilouy@sharif.edu (A. Hajilouy Benisi)

3D blade shape optimization to study the effects of an axial turbine stator and rotor blades stagger angle distributions on the pressure loading, mass flow rate and the turbine stage performance with two equivalent objective functions. The optimization is carried out at the turbine design point. To decrease the overall computational time, a novel method is implemented in the optimization algorithm based on grid independency consideration.

The paper is prepared as follows: In Section 2, the methods of optimization algorithm and flow simulation are discussed. The objective functions, aerodynamic shape representation and test facilities are introduced in this section as well. Section 3 contains results and discussion as well as the validations of the numerical solution scheme. A summary of the paper and main conclusions are finally presented in Section 4.

2. Methodology

In this section, the components of the paper, such as objective functions, shape representation, flow simulation method, test facilities and optimization algorithm, are presented in detail.

2.1. Objective functions

The optimization objective function is derived as a weighted sum of all individual objectives and is penalized with design constraints. In this paper, the individual objectives are the turbine isentropic efficiency and pressure ratio. In this investigation, two equivalent objective functions are considered. A constraint and an unconstraint form of objective function are studied to introduce the ability of direct search method. An axial turbine in constant mass flow rate and rotational speed is considered in the first case. To maximize its pressure ratio and efficiency, the first objective function is defined as:

$$F_{\text{obj}-1}\left(\vec{X}\right) = \min\left[C_1\frac{1-\eta_{tt}}{1-\eta_{tt}^*} + C_2\frac{\text{Pr}_{tt}^*}{\text{Pr}_{tt}}\right], \tag{1}$$

where $\vec{X}$ is the vector of design variables, which include the stagger angle linear distribution slopes of stator and rotor blades and C_1 and C_2 are constants prescribed by the designer. For different design conditions, C_1 and C_2 are specified appropriately. In this research, $C_1 = C_2 = 0.5$ in order to increase pressure ratio and efficiency simultaneously. In Eq. (1), the turbine isentropic efficiency and total-to-total pressure ratio are normalized by their original values, $\eta_{tt}^* = 90.08\%$ and $\text{Pr}_{tt}^* = 1.83$, respectively.

The balance of the turbine and the compressor power is considered as a constraint in the second objective function, given below, and while maximizing the turbine total-to-total efficiency, the generated power is allowed to change within 1%:

$$F_{\text{obj}-2}(X) = \min\left[\frac{1-\eta_{tt}}{1-\eta_{tt}^*} + \text{PT}\right],$$

$$\text{PT} = 5 \qquad \text{when} \quad \left|\frac{\dot{W}-\dot{W}^*}{\dot{W}^*}\right| > 0.01,$$

$$\text{otherwise} \quad \text{PT} = 0. \tag{2}$$

This objective function is penalized by the operating constraint. The optimization is accomplished by modifying the turbine blades span-wise stagger angle distribution while the blade profiles thickness distribution is kept constant.

2.2. Shape representation

Geometry parameterization methods have attracted renewed interests in recent years. Based on the optimization objects, different blade shape representations were used in various investigations, which are summarized in Table 1.

In the present paper, the original turbine geometry is given as set of x- and y-coordinates of several 2D airfoil sections at five and six span-wise locations for the rotor and stator blades, respectively. For optimization procedure, the 2D profiles are kept fix. Then, airfoil sections are stacked in order to create the 3D blade shape [19]. Finally, the span-wise stagger angle distribution is chosen to twist the profiles from

Table 1. Different blade shape representation.

Researchers	Curves	Applications
Oyama et al. [4]	B-spline curves	NASA rotor 67, mean camber line and thickness distribution
Luo et al. [5]	Non-uniform B-spline curves	NASA rotor 37, suction surfaces
Kim et al. [9]	Bezier curves	Centrifugal compressor, meridional plane
Lotfi et al. [10]	Bezier spline curves	Axial fan blades, camber line
Arabnia & Ghaly [3,13]	Quadratic rational Bezier curves	Axial turbine, stacking line distribution
Yuan et al. [16]	Non-uniform rational B spline	Steam turbine, blade stacking line
Komarov et al. [17]	Bezier curves	Axial compressor, suction and pressure sides
Büche [18]	B-spline curves	Axial compressor blade

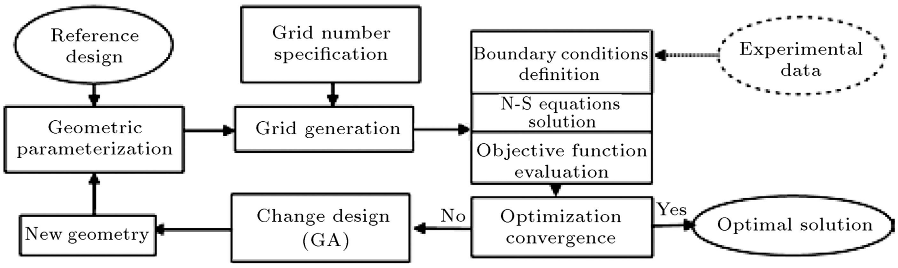

Figure 1. The flow chart of aerodynamic optimization processt.

Table 2. Geometrical specifications of the turbine blade.

Blade parameter	Stator	Rotor
Stagger angle at mean diameter (degree)	37	28
Inlet metal angle (degree)	15	22
Outlet metal angle (degree)	63	51
Hub diameter to axial chord at mean diameter	3.44	7.8
Tip diameter to axial chord at mean diameter	5.53	11.74
Pitch to chord at mean diameter	0.5	0.64
Aspect ratio	0.85	1.74

hub to tip. The goal is to improve an existing design scheme of the turbine with a simple representation of stagger angle distributions. The original stagger angle distribution is constant for the stator blades and increases linearly from hub to tip for the rotor ones.

2.3. Optimization algorithm

In this paper, the design optimization algorithm involves three basic steps: shape changing using rotation matrix, numerical optimization algorithm using GA, and flow simulation using RANS solver. The flow diagram of the calculation is shown in Figure 1. The optimizer evaluator uses the results of CFD analysis to calculate the fitness of each individual. The "reference design" in Figure 1 contains primary geometry. The experimental data are used for definition of required boundary conditions. The 3D coordinates of the original and modified geometries are fed to this optimization procedure as text files.

The GA optimizer involves 15 individuals per generation, the values of 0.15 and 0.8 for mutation and crossover probabilities. Two elite individuals were selected for passing to the next generation. Moreover, the method of Roulette wheel is employed for selecting pair of parents.

2.4. Flow simulation method

2.4.1. Geometry definition

In this investigation, numerical analysis is used to study the 3D flow field inside the turbine stage. The turbine stator is shrouded and the rotor tip clearance is 3.34% of its axial chord at mean diameter, which is considered as a part of computational domain. Several geometrical features of the turbine stage are given in Table 2.

2.4.2. Mesh generation

The structured elements generated on one pitch of the blades are shown in Figures 2 and 3. The mesh sizes in simulations are based on grid-independency considerations. To accelerate GA convergence rate,

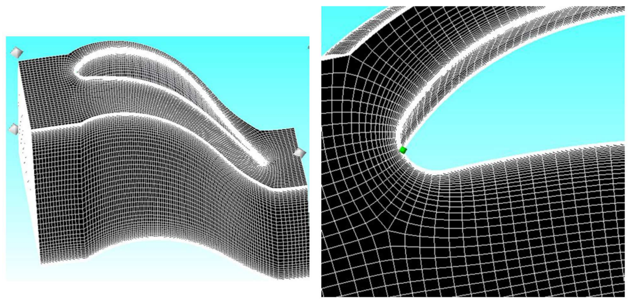

(a) (b)

Figure 2. Structured grid on the axial turbine stator surfaces (a) and stator leading edge (b).

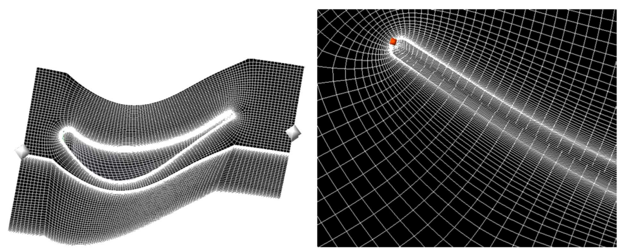

(a) (b)

Figure 3. Structured grid on the axial turbine rotor surfaces (a) and rotor trailing edge at tip surface (b).

Table 3. Grid independency consideration, efficiency and pressure ratio versus number of elements.

Generation	Number of elements specified		Number of elements generated		Output			Error (%)	
	Stator	Rotor	Stator	Rotor	Time (s)	Efficiency	Pressure ratio	Efficiency	Pressure ratio
1,2	200000	250000	202419	210540	986	89.68	1.829	0.44	0.00
3,4	300000	400000	296016	320778	1165	89.77	1.830	0.34	0.05
5,6	350000	500000	353649	440310	1396	89.83	1.834	0.28	0.27
7,8	400000	600000	396614	531470	1547	89.85	1.833	0.26	0.22
9,10	450000	700000	439552	664481	1876	90.06	1.830	0.02	0.05
11-16	700000	800000	675150	746448	2050	90.08	1.829	0.00	0.00
—	800000	900000	793026	865311	2529	90.08	1.829	0.00	0.00

the number of computational elements are increased from coarse grids to fine, in each generation, based on grid independency study. Euler and RANS solutions on coarse grids are sometimes proposed as meta-functions [20]. In this optimization study, this approximation method is fast and accurate, because of the data which is given in Table 3. In this table, the required time for each level of generation is given. In each two-generation sets, a pre-specified number of elements are considered. The error values, for pressure ratio and efficiency are calculated based on the values, which were obtained in the final study. Using this method, the overall computational time decreases by 20%. All computations are performed on a 3.5GHz core I7 PC. The "grid number specification" in Figure 1 is based on the values given in Table 3.

2.4.3. Numerical method

In this paper, 3D and steady state flow simulations are carried out by a 3D solver. The RANS equations are solved by means of a finite volume method [21]. The Reynolds stress terms in the momentum transport equations are solved using the SST turbulence model [22,23]. Based on the number of elements specified in each generation, the turbine blade domains are meshed and then the iterative procedure is started by the N-S equations solver. The maximum residual convergence criterion is set to be 10^{-5}. Convergence is met when the average errors reach the specified limit and the ratio of inlet to the outlet mass flow is equal to unity. It should be mentioned that the mixture of combustion products is defined as the working fluid.

2.4.4. Boundary conditions

The boundary conditions for simulations are:

1. Mass flow rate and total temperature values are specified to the axial turbine inlet with no pre-swirl, as well as the turbulence intensity;
2. Average static pressure value is imposed at the outlet of the turbine, based on experimental measurement;
3. Adiabatic (stationary or moving) walls, zero velocity or no slip boundary condition, is considered for blade surfaces;
4. Mixing plane condition is used for interfaces among the axial turbine stator and rotor;
5. Because of circumferential symmetric geometry, periodic boundary condition is used for the simulation.

2.5. Test facilities

Experimental studies are performed at Gas Turbine Laboratory of Sharif University of Technology, where a single shaft gas turbine is investigated. The schematic of experimental arrangements, used in this research, is shown in Figure 4. The gas turbine rotational speed and air mass flow rate values are measured via a magnetic pickup and a bell-mouth at the inlet, respectively. Measuring the static pressure and temperature in the bell-mouth throat section, the gas turbine mass flow rate is calculated by:

$$\dot{m} = C\frac{P}{RT}A\sqrt{2C_P(T_0 - T)}. \tag{3}$$

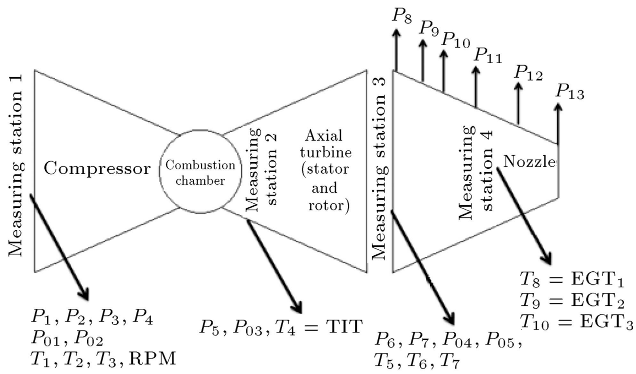

Figure 4. The schematic of experimental arrangement [25,26].

Table 4. The turbine design point conditions.

Inlet total temperature (K)	1130
Stage total pressure ratio	1.83
Mid-span flow coefficient	0.88
Total-to-total efficiency (%)	90.08
Mid-span stage loading	5.15
Average reaction (%)	28.5

To perform the experimental measurements, the gas turbine engine is installed on the test rig, and all the connections of the accessories including fuel, compressed air and oil pump are linked to the gas turbine. Then, the measurement instruments are connected. After starting the engine, the gas turbine accelerates to the pre-specified rotational speed in several steps [24]. More details of this test rig are given elsewhere [25,26].

3. Results and discussion

In this section, the optimization scheme, numerical and experimental procedures described in the previous section are applied for a single stage axial turbine. The numerical optimization is performed at the turbine design condition, which is provided in Table 4.

3.1. Performance verification

The axial turbine pressure ratio and isentropic efficiency versus the rotational speed are obtained from the experimental results, which are used for validation of 3D numerical simulation results. In Figure 5, the experimental pressure ratios of the axial turbine are presented versus the rotational speed. The numerical simulation results at five different rotational speeds are compared with these experimental results. The maximum difference is 2%.

Some numerical and experimental results of total-to-total and total-to-static isentropic efficiency are given in Table 5. The maximum deviation is around 2.48%.

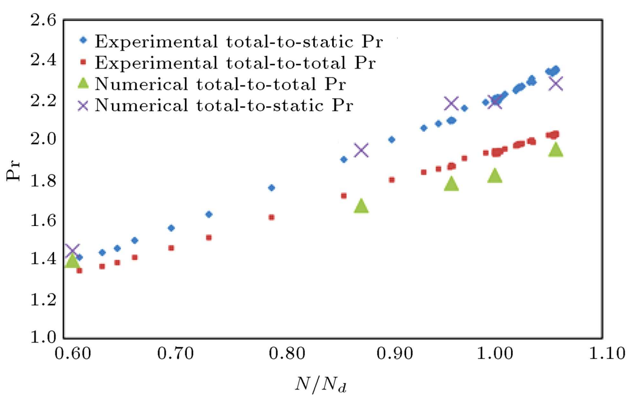

Figure 5. Pressure ratio versus normalized rotational speed, experimental and numerical results of the axial turbine.

3.2. Optimum stagger angle distribution of axial turbine

The blade stagger angle distribution influences rather strongly the span-wise variation of mass flow, incidence and throat area, hence, the 3D flow features. The stator stagger distribution is usually approximated by a constant value, while the rotor stagger distribution takes a linear form from hub to tip. It is worth to mention that these functionalities are not necessarily optimum ones.

In Figure 6, the optimization histories for the first and second objective functions are shown. In this figure, total-to-total efficiencies of different redesigned turbines versus total-to-total pressure ratios

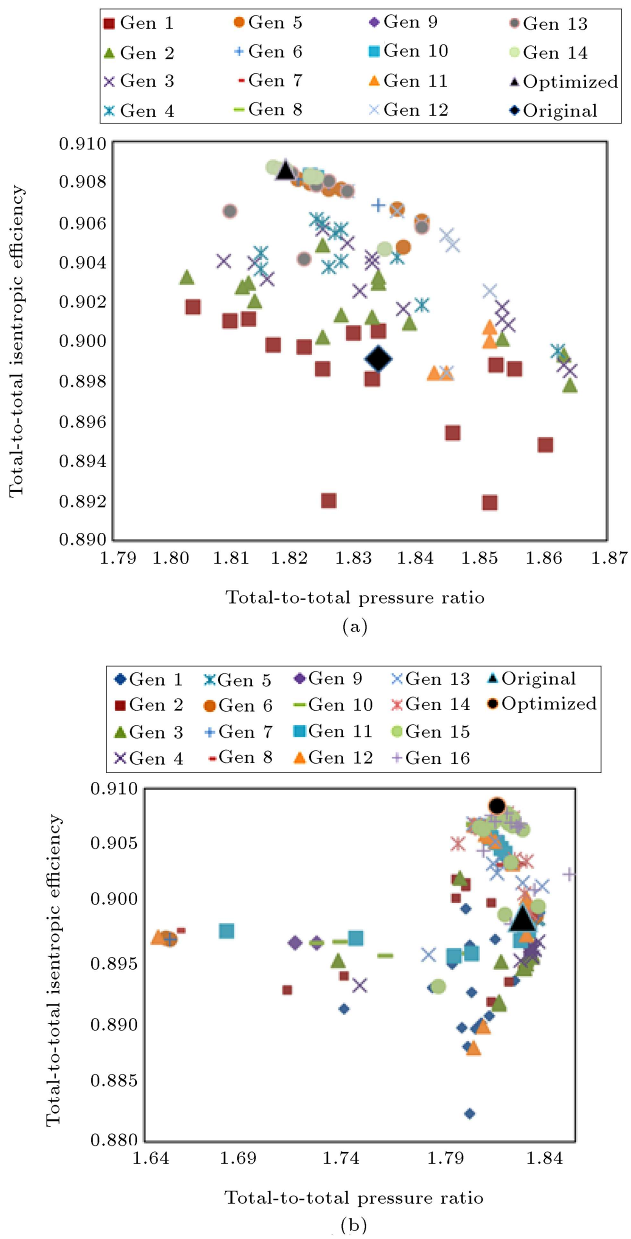

Figure 6. Optimization history in (a) case 1, and (b) case 2 (Gen = GA generation).

Table 5. Numerical and experimental results of total-to-total and total to static isentropic efficiency [25,26].

		Numerical	Experimental	Deviation (%)
Total-to-total efficiency	At design speed, $N = N_d$	90.08	87.9	2.48
	At off-design speed, $N = 1.05N_d$	90.4	88.9	1.6
Total to static efficiency	At design speed, $N = N_d$	67.9	67.1	1.2
	At off-design speed, $N = 1.05N_d$	67.9	67.2	1

Table 6. Original and optimum turbine performance parameters.

Case	Pr	Efficiency	Change in Pr (%)	Change in efficiency (%)
Original	1.829	90.08	-	-
1	1.818	90.86	-0.60	0.86
2	1.82	90.85	-0.49	0.85

at a single operating point are shown. The GA provides higher efficiency but lower pressure ratio after 14 or 16 generations. At the optimum point, the objective function value is equal to 0.964 and 0.92 in cases 1 and 2, respectively. The original and optimum turbine stage performance parameters and the corresponding range of variations are given in Table 6, which shows that two different formulations of objective functions, (Eqs. (1) and (2)), yield nearly similar optimization results. In this optimization procedure, it is possible to consider un-constrained and constrained objective functions. In this paper, keeping the mass flow rate and the inlet total temperature fixed, the turbine-generated power is directly related to the pressure ratio. Under such conditions, the turbine generated power increases through increasing the pressure ratio, as given by:

$$\dot{W} = \dot{m}C_P\left(T_{0\text{in}} - T_{0\text{out}}\right) = \dot{m}C_P T_{0\text{in}}\left(1 - \frac{T_{0\text{out}}}{T_{0\text{in}}}\right)$$
$$= \dot{m}C_P T_{0\text{in}}\left(1 - (\mathrm{Pr}^{-1})^{\frac{\gamma-1}{\gamma}}\right) \Rightarrow \mathrm{Pr}$$
$$= \left(1 - \frac{\dot{W}}{\dot{m}C_P T_{0\text{in}}}\right)^{\frac{-\gamma}{\gamma-1}}, \qquad \text{where} \quad \mathrm{Pr} = \frac{P_{0\text{in}}}{P_{0\text{out}}}. \tag{4}$$

In Figure 7, the span-wise stagger angle distributions of stator and rotor blades are shown for original and modified turbines. In the present work, the rotor and stator stagger angles are allowed to change linearly from hub to tip with two design variables, which are the slopes of stator and rotor linear distributions. The rotor and stator mid-span stagger angles are not changed during the optimization procedures. The optimum stagger angles, in both cases, decrease near the hub and increase near the tip, by an equal amount; see Figure 7(a). On the other hand, the rotor stagger

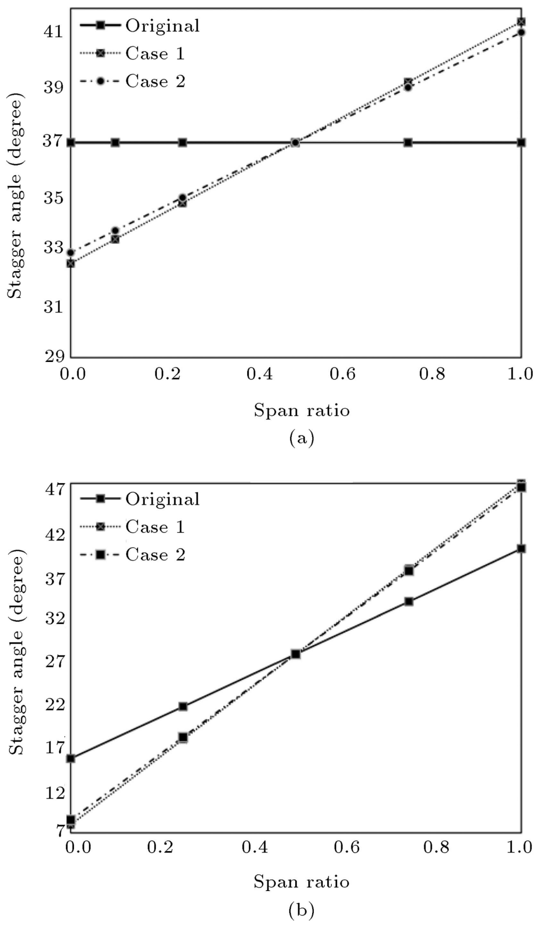

Figure 7. Original and modified stagger angle distribution: (a) stator; and (b) rotor.

angles vary in the same trend with different amounts as shown in Figure 7(b).

The stator and rotor blades re-staggering affects the spanwise loading variations, as shown in Figures 8 and 9 for the stator and rotor blades, respectively. In these figures, the pressure loading distributions in three spans of blades, near the hub, mid-span and near the tip cross sections, are shown. The pressure loading is defined as the difference of pressure forces acting on the pressure and suction surfaces of the blade. As a result, the area of the closed surfaces in Figures 8 and 9 is a suitable estimation of pressure loading in each cross section. According to Figure 8, the stator hub, mid and tip profiles have higher loading in both cases in comparison with the original case. The

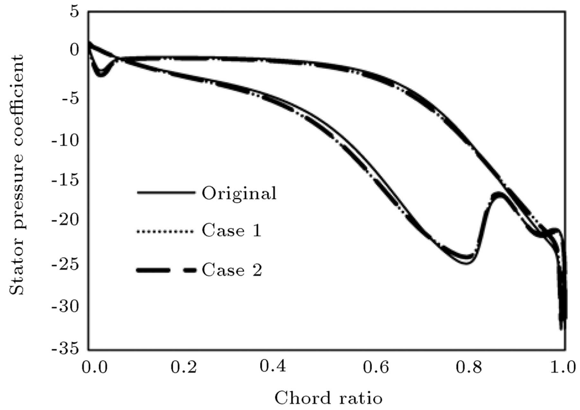

(a)

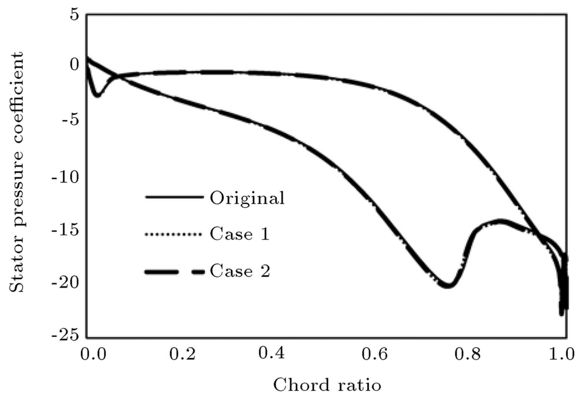

(b)

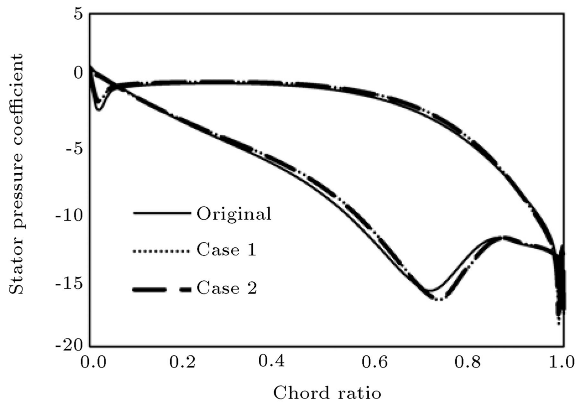

(c)

Figure 8. Stator blade surface pressure distribution at (a) hub, (b) mid-span, and (c) tip.

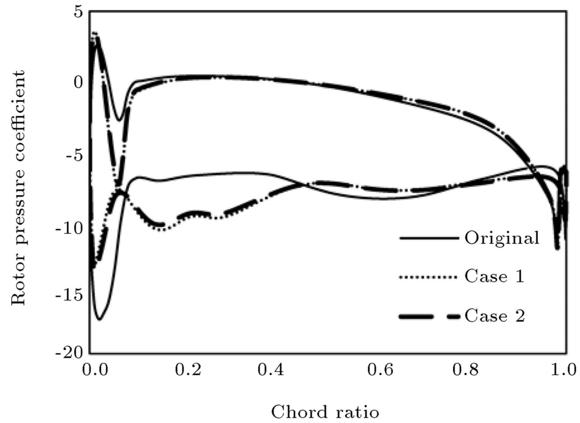

(a)

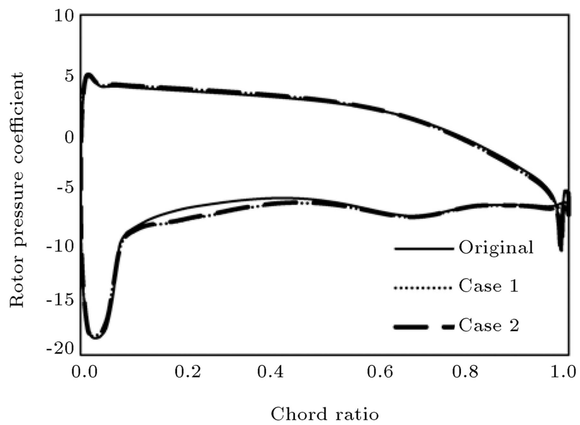

(b)

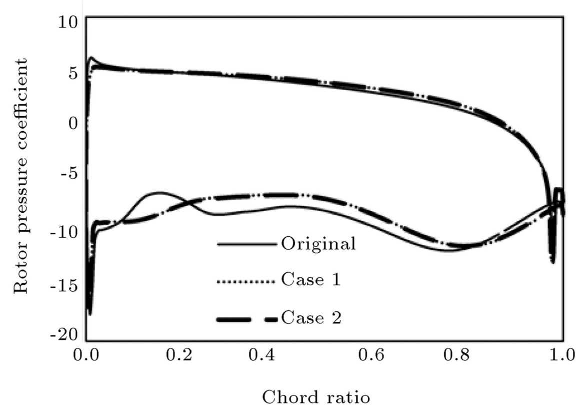

(c)

Figure 9. Rotor blade surface pressure distribution at (a) hub, (b) mid-span, and (c) tip.

maximum increase of pressure loading is 2.74% in hub cross section.

The rotor pressure distribution in the hub cross section varies considerably due to changes of the stator and rotor stagger angle in this section, as in Figure 9(a), which causes higher loading in cases 1 and 2 compared to the original turbine. The maximum increase is 6.15% in case 2.

Figure 9(b) shows rotor pressure distribution in mid-span surface which obtained around 4.0% increase in pressure loading in both cases. The tip profiles have lower loading in both cases, as shown in Figure 9(c). The maximum decrease in tip cross section loading is 2.2%. Due to the lower pressure loading in rotor tip cross section, the optimized geometry leads to lower tip leakage, which is desired.

In Figure 10, span-wise variation of stator and rotor exit mass flows is shown. When the stator stagger angles vary according to Figure 7(a), mass flow rate

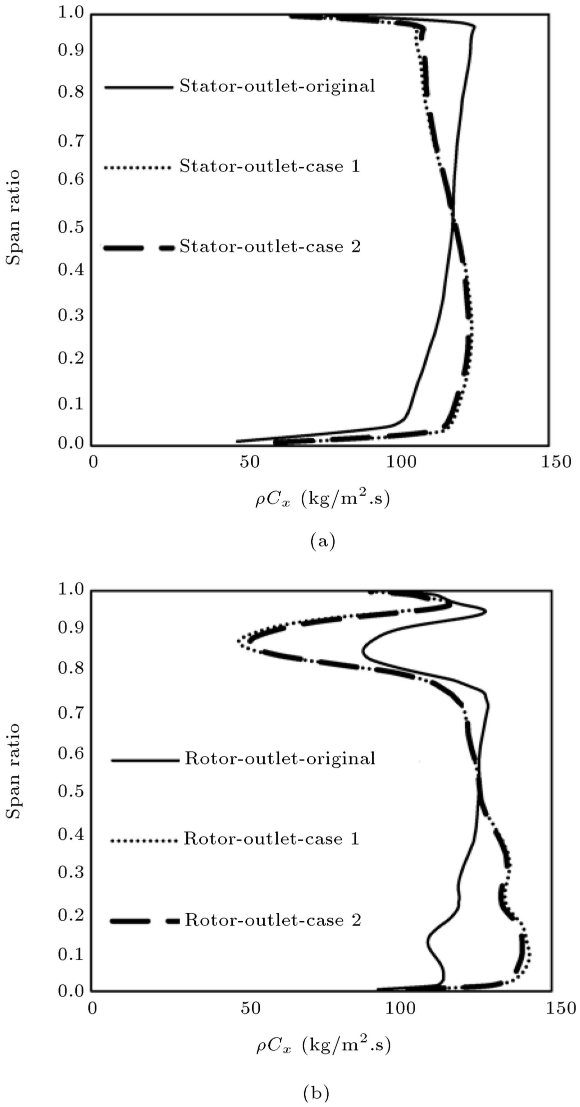

Figure 10. Span-wise variation of mass flow in original, case 1 and case 2 turbines; stator (a) and rotor (b) exits.

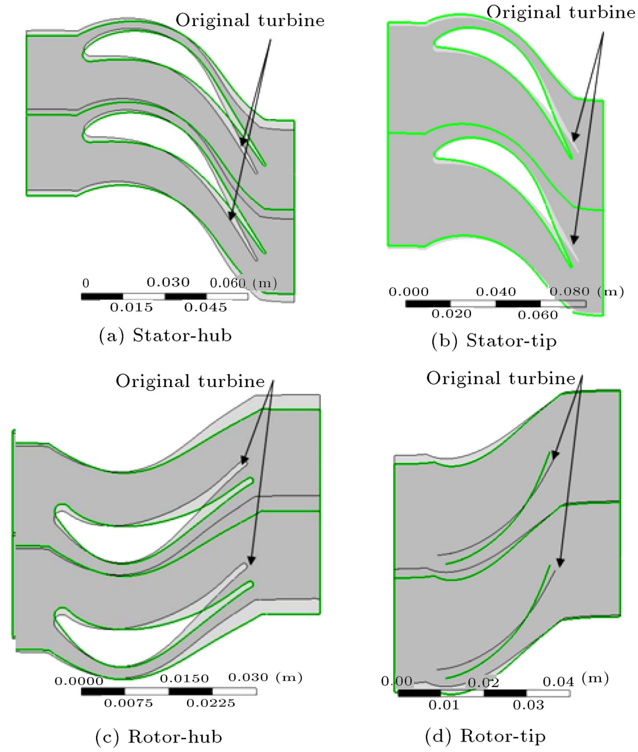

Figure 11. The changes of stagger angle in original and modified turbine hub and tip surfaces.

from the hub to the mid-span increases while up to the tip decreases, in both cases. This variation affects the mass flow rate at rotor inlet and outlet as well (see Figure 10(b)) with similar trends. Figure 10(a) shows that calculated mass flow profiles downstream of the stator are nearly uniform except near the end walls, while, those of the rotor blade are highly distorted by the effects of secondary flows.

A higher blade stagger angle implies a smaller throat area and hence less mass flow rate, as illustrated in Figures 10 and 11. In stator and rotor hub cross sections, the stagger angle decrease and vice versa near the tip. These variations are shown in Figure 11(a) to (d).

The optimization procedure is carried out at single operating point for both cases. To investigate the performance of the modified turbines in other operating conditions, the turbine characteristic curves at design speed are obtained. In Figure 12(a) and (b), original and modified turbine stage mass parameters as well as total-to-total efficiencies versus pressure ratios are depicted, respectively. While the maximum decrease in mass parameter in choke condition is 0.72%, the maximum increase in turbine efficiency are 0.86% and 0.85% in cases 1 and 2, respectively.

4. Summary and conclusions

The 3D optimization method is a useful tool for design of high performance axial turbine blades. The main objective of this research is to use the 3D shape optimization to study the effects of turbine stator and rotor blades stagger angle variations on the turbine stage performance with two objective functions. The span-wise blade stagger angle distribution is manipulated to optimize the aerodynamic performance of the turbine. Geometry candidates for the optimization algorithm are generated by re-staggering the 2D airfoil sections. Gas turbine engine experimental measurements are used for defining the boundary conditions as well as validation of simulations. The numerical method employed in this research, combines a genetic algorithm significantly accelerated using a coarse to fine grids and a verified numerical solver. In this optimization, the stator and rotor hubs stagger angles decrease from 37° to 32.5° and from 15° to 7°, whereas

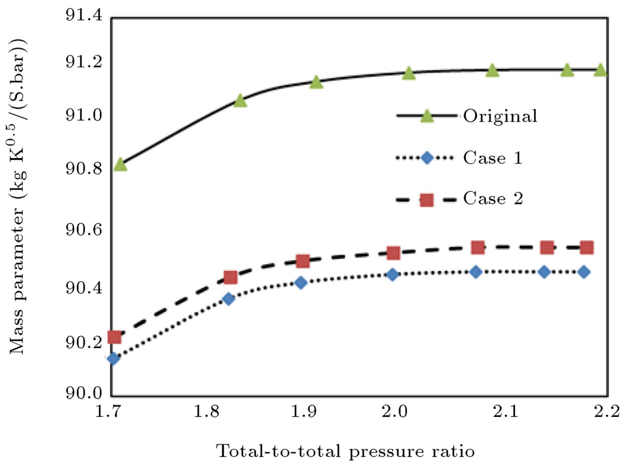

(a)

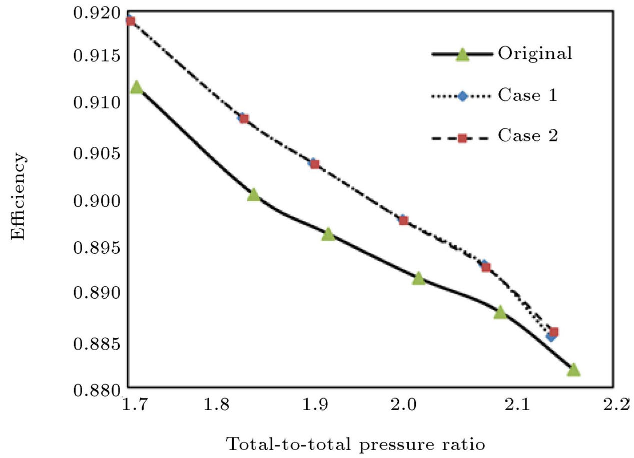

(b)

Figure 12. The original and modified turbine stage mass parameters (a) and total-to-total efficiency (b) versus pressure ratio at $N = N_d$.

those of the tips increase from 37° to 41.5° and from 40° to 47°, respectively. The optimization strategy results in a valuable improvement of 0.86% in the turbine stage efficiency, increasing that from 90.08% to 90.86%.

Acknowledgments

The authors gratefully acknowledge the support of research and technology office at Sharif University of technology as well as Gas Turbine Lab staff.

Nomenclature

A	Bell-mouth area (m^2)
C	Correction coefficient
C_1, C_2	Weights of objective function
CP_r	Rotor pressure coefficient $= \frac{P-P_{\text{in}}}{0.5\rho_{\text{in}} V^2_{\text{in, rel}}}$
CP_s	Stator pressure coefficient $= \frac{P-P_{\text{in}}}{0.5\rho_{\text{in}} V^2_{\text{in}}}$
C_P	Specific heat capacity at constant pressure (Jkg^{-1}.K^{-1})
C_x	Axial velocity in stationary frame (m.s^{-1})
F	Objective function
$\dot{m}$	Mass flow rate (kg/s)
Mp	Mass parameter $= \dot{m}\sqrt{T_{0\text{in}}}/P_{0\text{in}}$ (kg$\sqrt{\text{K}}$/s.bar)
N	Rotational speed of gas turbine (RPM)
P	Pressure (kg.m^{-1}.s^{-2})
Pr$_{tt}$	Total pressure ratio $= P_{0\text{in}}/P_{0\text{out}}$
PT	Penalty Term
T	Temperature (K)
R	Specific gas constant (J.kg^{-1}.K^{-1})
$\dot{W}$	Turbine output power (W)
X	Vector of design variables

Greek symbols

ρ	Density (kg.m^{-3})
η_{tt}	Turbine total-to-total isentropic efficiency

Superscript

$*$	Original turbine values

Subscripts

0	Stagnation property
d	Design point
in	Inlet
obj	Objective function
out	Outlet
r	Rotor
rel	Relative
s	Stator
t	Total property

Acronyms

CFD	Computational Fluid Dynamics
GA	Genetic Algorithm
RANS	Reynolds-Averaged Navier-Stokes
SST	Shear Stress Transport
2D	Two-Dimensional
3D	Three-Dimensional

References

1. Rezasoltani, M., Schobeiri, M.T. and Han, J.C. "Experimental investigation of the effect of purge flow on film cooling effectiveness on a rotating turbine with non-axisymmetric endwall contouring", *Proceeding of ASME Turbo Expo*, San Antonio, Texas (2013).

2. Pierret, S. "Multi-objective and multi-disciplinary optimization of three-dimensional turbo-machinery blades", *Proceedings of the 6th World Congresses of Structural and Multidisciplinary Optimization* (2005).

3. Arabnia, M. and Ghaly, W. "A strategy for multi-point shape optimization of turbine stages in three-dimensional flow", *Proceeding of ASME Turbo Expo*, Orlando, Florida, USA (2009).

4. Oyama, A., Liou, M.S. and Obayashi, S., *Transonic Axial Flow Blade Shape Optimization Using Evolutionary Algorithm and Three-Dimensional Navier-Stokes Solver*, Citeseer, **4** (2002).

5. Luo, C., Song, L., Li, J. and Feng, Z. "Multi-objective optimization approach to multidisciplinary design of a three-dimensional transonic compressor blade", *Proceeding of ASME Turbo Expo*, Orlando, Florida, USA (2009).

6. Okui, H., Verstraete, T., Van den Braembussche, R.A. and Alsalihi, Z. "Three dimensional design and optimization of a transonic rotor in axial flow compressors", *Proceeding of ASME Turbo Expo*, Vancouver, British Columbia, Canada (2011).

7. Benini, E. "Three-dimensional multi-objective design optimization of a transonic compressor rotor", *Int. J. of Propulsion and Power*, **20**(3), pp. 559-565 (2004).

8. Nili-Ahmadabadi, M., Durali, M. and Hajilouy-Benisi, A. "A novel quasi 3-D design method for centrifugal compressor meridional plane", *Proceeding of ASME Turbo Expo*, Glasgow, UK (2010).

9. Kim, J.H., Choi, J.H. and Kim, K.Y. "Design optimization of a centrifugal compressor impeller using radial basis neural network method", *Proceeding of ASME Turbo Expo*, Orlando, Florida, USA (2009).

10. Lotfi, O., Teixeira, J.A., Ivey, P.C., Kinghorn, I.R. and Sheard, A.G. "Shape optimization of axial fan blades using genetic algorithms and a 3D Navier-Stokes solver", *Proceeding of ASME Turbo Expo*, Barcelona, Spain (2006).

11. Jin, H. "Design of a highly loaded transonic two-stage fan using swept and bowed blading", *Proceeding of ASME Turbo Expo*, Vancouver, British Columbia, Canada (2011).

12. Yershov, S., Rusanov, A., Shapochka, A., Lampart, P., Wirydczuk, J. and Gardzilewicz, A. "Shape optimization of two turbine stages using the deformed polyhedron method and a three-dimensional RANS solver", *Proc. IMechE, Part A: J. of Power and Energy*, **216**(2), pp. 203-213 (2002).

13. Arabnia, M. and Ghaly, W. "On the use of blades stagger and stacking in turbine stage optimization", *Proceeding of ASME Turbo Expo*, Glasgow, UK (2010).

14. Sivashanmugam, V.K., Arabnia, M. and Ghaly, W. "Aero-structural optimization of an axial turbine stage in three-dimensional flow", *Proceeding of ASME Turbo Expo*, Glasgow, UK (2010).

15. Arabnia, M., Sivashanmugam, V.K. and Ghaly, W. "Optimization of an axial turbine rotor for high aerodynamic inlet blockage", *Proceeding of ASME Turbo Expo*, Vancouver, British Columbia, Canada (2011).

16. Yuan, X., Tanuma, T., Zhu, X., Lin, Z. and Nomura, D. "A CFD approach to fluid dynamic optimum design of steam turbine stages with stator and rotor blades", *Proceeding of ASME Turbo Expo*, GT2010-22477 (2010).

17. Komarov, O.V., Sedunin, V.A. and Blinov, V.L. "Application of optimization techniques for new high-turning axial compressor profile topology design", *Proceedings of ASME Turbo Expo 2014: Turbine Technical Conference and Exposition*, Düsseldorf, Germany (2014)

18. Büche, D., Guidati, G. and Stoll, P. "Automated design optimization of compressor blades for stationary, large-scale turbomachinery", *Proceeding of ASME Turbo Expo*, Atlanta, Georgia, USA (2003).

19. Moustapha, H., Zelesky, M.F., Baines, N.C. and Japikse, D. "Axial and radial turbines", Concepts NREC, pp. 97-110 (2003).

20. Van den Braembussche, R.A., *Numerical Optimization for Advanced Turbomachinery Design. Optimization and Computational Fluid Dynamics*, pp. 147-189 (2008).

21. Mojaddam, M., Hajilouy Benisi, A. and Movahhedi, M.R. "Optimal design of the volute for a turbocharger radial flow compressor", *Proc. IMechE, Part G: J. of Aerospace Engineering* (2014). DOI: 10.1177/0954410014542448

22. Wilcox, D.C. "Turbulence modeling for CFD", *AIAA*, **2**, DCW Industries La Canada, CA (1998).

23. Menter, F.R. "Two-equation eddy-viscosity turbulence models for engineering applications", *AIAA Journal*, **32**(8), pp. 1598-1605 (1994).

24. Karrabi, H., Pourfarzaneh, H. and Hajilouy-Benisi, A. "Zero D and 3D analysis of the centrifugal compressor of a gas turbine and its evaluation using experimental results", *ASME 2011 International Mechanical Engineering Congress and Exposition:* American Society of Mechanical Engineers, pp. 897-906 (2011).

25. Asgarshamsi, A., Hajilouy Benisi, A., Assempour, A. and Pourfarzaneh, H. "Multi point optimization of lean and sweep angles for stator and rotor blades of an axial turbine", *Proceedings of ASME Turbo Expo 2014: Turbine Technical Conference and Exposition*, Düsseldorf, Germany (2014).

26. Asgarshamsi, A., Hajilouy Benisi, A., Assempour, A. and Pourfarzaneh, H. "Multi-objective optimization of lean and sweep angles for stator and rotor blades of an axial turbine", *Proc. IMechE, Part G: J. of Aerospace Engineering* (2014). DOI: 10.1177/0954410014541080

Biographies

Abolhassan Asgarshamsi obtained his BS degree in Mechanical Engineering from University of Tehran, Iran, in 2006, and his MS degree in Mechanical Engineering from the Department of Mechanical Engineering at Sharif University of Technology, Tehran, Iran, in 2009. He is currently a PhD candidate at the same university. Mr. Asgarshamsi's research interests include optimization of turbomachinery systems and study of heat transfer in various equipments.

Ali Hajilouy-Benisi received his PhD degree from the Mechanical Engineering Department of Imperial College at the University of London in 1993. He has been faculty member of the Institute of Water and Energy and then the School of Mechanical Engineering at Sharif University of Technology (SUT) since 1978. He served as Director of the Fluid Mechanics Laboratory from 1993-1995, Founder and Director of the Turbocharger Laboratory from 1993, Founder and Director of the Turbocharging Laboratory from 2000, Founder and Director of the Gas Turbine Laboratory from 2008, at the School of Mechanical Engineering of SUT. His research interests are experimental and theoretical investigations of turbochargers, turbocharging, and gas turbines. He is author or co-author of over 90 conferences and journal papers, and coordinator for compiling and publishing four volumes research reports of SUT for 1991-1995. He has also supervised over 40 graduate theses. He has conducted more than seven research-funded projects.

Ahmad Assempour received his BS and MS degrees in Mechanical Engineering from Tehran Polytechnic University, Iran, in 1979 and 1985, respectively, and his PhD degree in Mechanical Engineering from Oklahoma State University, U.S.A. in 1989. He is now a professor at the School of Mechanical Engineering, Sharif University of Technology. His research interests include plasticity and mechanics of metal forming, modeling of sheet and bulk forming, and die design in auto stamping industries.